Supplement of Atmos. Chem. Phys., 24, 3197–3215, 2024
https://doi.org/10.5194/acp-24-3197-2024-supplement

Atmospheric Chemistry and Physics Open Access

Supplement of

Contribution of brown carbon to light absorption in emissions of European residential biomass combustion appliances

Satish Basnet et al.

Correspondence to: Satish Basnet (satish.basnet@uef.fi), Anni Hartikainen (anni.hartikainen@uef.fi), and Olli Sippula (olli.sippula@uef.fi)

Table S1. Dry fuel properties of fuel types used in experiments.

Parameter	birch log	birch log	birch log	birch log	beech log	spruce log	pine log	softwood pellets	peat
moisture (%)	7.20	11.0	18.0	28.0	9.00	7.40	6.10	7.30	17.9
ash content @ 550 °C (% (w/w, dry))	0.69	0.69	0.69	0.69	1.30	0.58	0.45	0.36	4.90
carbon (% (w/w, dry))	51.0	51.0	51.0	51.0	50.3	52.0	51.1	51.7	56.2
hydrogen (% (w/w, dry))	6.00	6.00	6.00	6.00	5.80	5.90	6.40	6.00	5.70
nitrogen (% (w/w, dry))	0.40	0.40	0.40	0.40	0.36	0.36	< 0.05	0.29	2.01
oxygen (% (w/w, dry))	41.9	41.9	41.9	41.9	42.3	41.1	42.0	41.6	-
sulphur (% (w/w, dry))	0.006	0.006	0.006	0.006	0.037	0.009	<0.005	0.006	0.22
chlorine (% (w/w, dry))	<0.005	<0.005	<0.005	<0.005	<0.005	0.005	<0.005	0.006	0.023
Net calorific value (MJ per kg fuel)	18.1	18.1	18.1	18.1	17.8	18.6	19.3	18.4	22.9

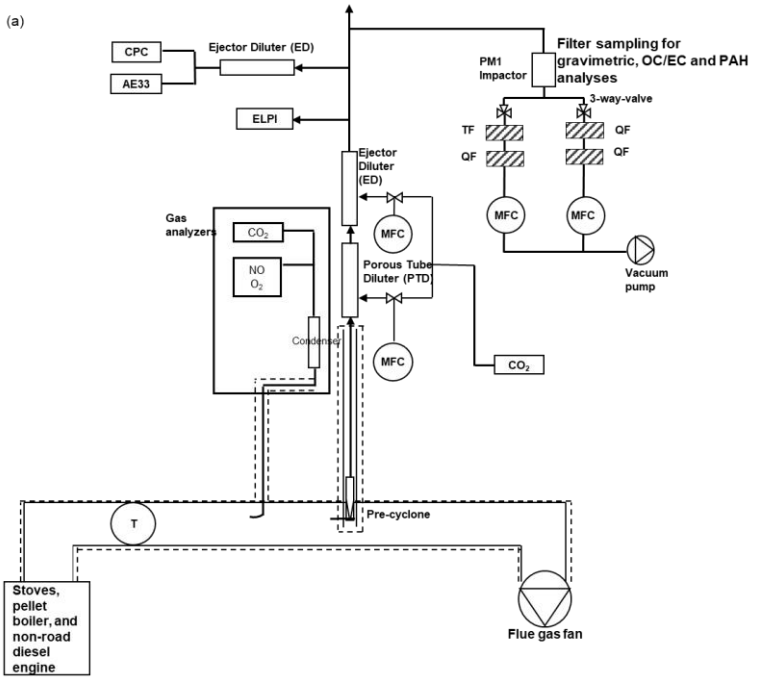

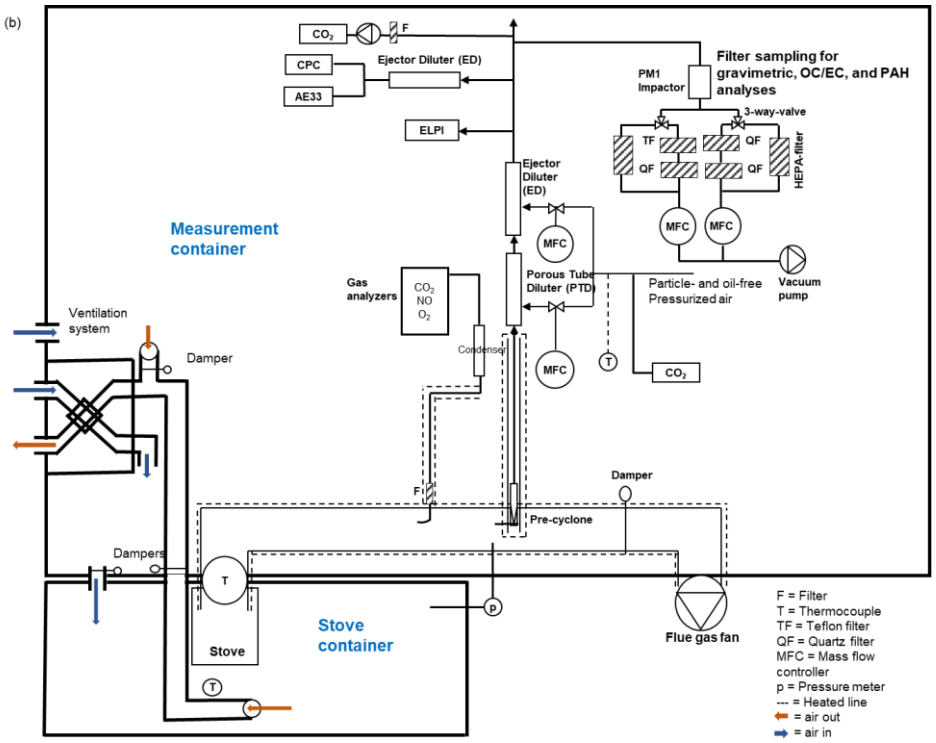

5

Figure S1. Schematics of the experimental setup at a) ILMARI and b) SIMO (modified from Tissari et al. (2019)).

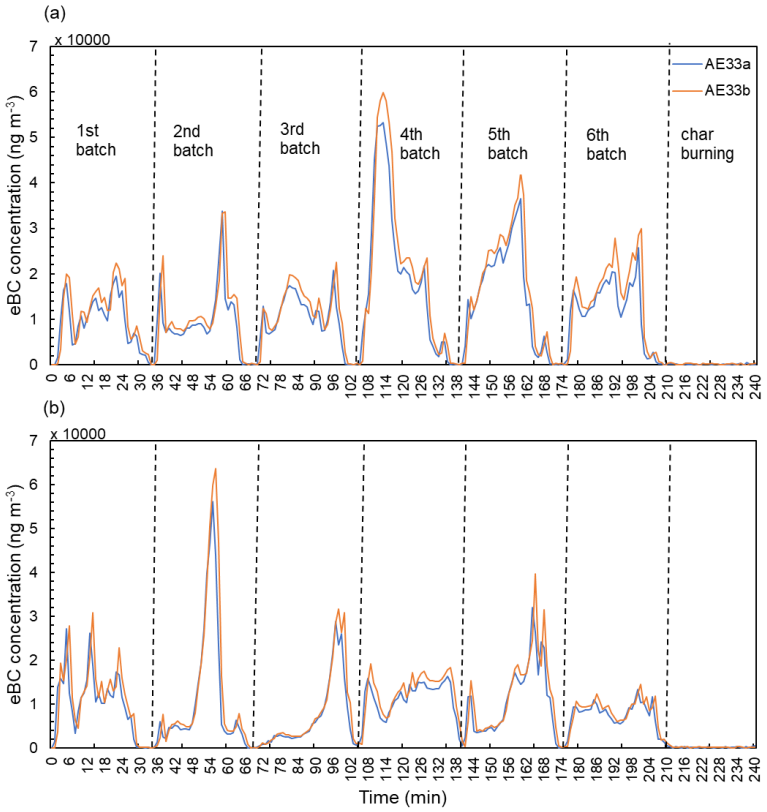

Figure S2. Comparison of black carbon concentration raw data between the two AE33 instruments used in this work. The concentrations are without DR correction and originate from two individual MCS experiments in ILMARI 2021 experiments.

Table S2. Fuel types burnt in different appliances along with the fuel moisture content, Air-to-fuel ratio, DR after the first dilution step, and modified combustion efficiency (MCE) are reported as averages (± average of SD during the experiments) for all experiments.

Appliance	Abbrv	Measurement site and date	fuel type	fuel moisture content	number of repetitions	number of batches	Air-to-fuel ratio	DR	MCE
Modern masonry heater	MMH	ILMARI 2013	beech	9 %	4	6	5.21 ± 1.47	37.4 ± 6.34	0.98 ± 0.02
			spruce	7.4 %	3	6	4.03 ± 0.65	37.3 ± 5.95	0.97 ± 0.04
			birch	7.2 %	6	6	3.84 ± 0.43	36.2 ± 3.37	0.98 ± 0.03
Conventional masonry heater	CMH	SIMO 2019	birch	11 %	3	3–4	2.82 ± 0.29	89.8 ± 0.20	0.98 ± 0.01
Sauna stoves (10 types)	SS-11	SIMO 2018	birch	11 %	23	3	2.55 ± 0.41	87.9 ± 7.91	0.97 ± 0.02
	SS-18		birch	18 %	12	3	2.81 ± 0.39	73.0 ± 17.8	0.95 ± 0.01
	SS-28		birch	28 %	3	3	2.68 ± 0.17	91.7 ± 2.52	0.94 ± 0.002

Modern chimney stove	MCS	ILMARI 2016	pine	6.1 %	3	5	2.79 ± 0.23	13.7 ± 0.49	0.98 ± 0.01
			spruce	7.4 %	3	5	2.76 ± 0.27	23.4 ± 7.29	0.98 ± 0.01
		ILMARI 2021	beech	9 %	14	6	2.37 ± 0.37	57.6 ± 7.78	0.98 ± 0.02
			peat	17.9 %	3	8	3.14 ± 0.46	101 ± 0.74	0.99 ± 0.01
Pellet boiler	PB	ILMARI 2016	softwood pellets	7.3 %	3	4	2.48 ± 0.53	10.1 ± 0.72	0.998 ± 0.002
Non-road diesel engine	NrDE	ILMARI 2016	diesel		3	4	3.35 ± 1.16	9.75 ± 1.24	0.998 ± 0.001

Section S1 Determination of the BrC fraction

The contribution of brown carbon to the total aerosol absorption ($BrC_{370\text{-}950}$) was calculated based on the absorption coefficients measured by the seven-wavelength aethalometer. Using the experiment-type-wise averaged absorption coefficients, we establish parameters labelled total dimensionless integrated absorption of the total aethalometer wavelength range (DIA_{Tot}), BC (DIA_{BC}), and BrC (DIA_{BrC}). In the following, this calculation is presented step-by-step first in general, then for a specific example case of a modern chimney stove (MCS).

a) Determination of the total dimensionless integrated absorption (DIA_{Tot}). A power law function is fit to the absorptions measured at the seven aethalometer wavelengths using the least squares method.

$$b_{abs,fit}(\lambda) = B_{abs,fit}(880nm) \times \left(\frac{\lambda}{880\ nm}\right)^{-AAE_{370-950}} \quad \text{(S1)}$$

Where $B_{abs,fit}(880nm)$ represents the absorption by BC at 880 nm, with the unit m^{-1}. DIA_{tot} is then computed as the definite integral over the wavelength range of λ_1 = 370 nm to λ_2 = 950 nm.

$$DIA_{Tot} = \int_{\lambda_1}^{\lambda_2} B_{abs,fit}(880nm) \times \left(\frac{\lambda}{880\ nm}\right)^{-AAE_{370-950}}\ d\lambda = \frac{B_{abs,fit}(880nm) \times 880\ nm^{\,AAE_{370-950}}}{-AAE_{370-950}+1} \times (950\ \text{nm}^{-AAE_{370-950}+1} - 370\ \text{nm}^{-AAE_{370-950}+1}) \quad \text{(S2)}$$

b) Determination of the dimensionless integrated absorption by BC (DIA_{BC}) by computing the definite integral of the BC function (eq. S3) over the wavelength range of 370 nm to 950 nm. Here, an AAE_{BC} of 1 was applied.

$$b_{abs}(BC,\lambda) = b_{abs}(880nm) \times \left(\frac{\lambda}{880\ nm}\right)^{-AAE_{BC}} \quad \text{(S3)}$$

$$DIA_{BC} = \int_{\lambda_1}^{\lambda_2} b_{abs}(880nm) \times \left(\frac{\lambda}{880\ nm}\right)^{-1} d\lambda\ = b_{abs}(880nm) \times 880\ nm \times \ln\left(\frac{950nm}{370nm}\right) \quad \text{(S4)}$$

c) Determination of the dimensionless integrated absorption by BrC (DIA_{BrC}) as the difference between DIA_{Tot} and DIA_{BC}.

$$DIA_{BrC} = DIA_{Tot} - DIA_{BC} \quad \text{(S5)}$$

d) The total contribution of brown carbon to the aerosol absorption ($BrC_{370\text{-}950}$) is then defined as the ratio of DIA_{BrC} to DIA_{Tot}.

$$BrC_{370-950} = \frac{DIA_{BrC}}{DIA_{Tot}} \quad \text{(S6)}$$

Example calculation: The calculation of the DIAs demonstrated in Figure S3(a–c) for the case of MCS use.

The total absorption is represented by the following function: $b_{abs}(\lambda) = 0.55\ m^{-1} \times \left(\frac{\lambda}{880\ nm}\right)^{-1.201}$, as illustrated in Figure S3a. Integrating this function over the wavelength range of 370 nm to 950 nm, as shown in Eq. (S2), we get the DIA_{Tot} of 495.5 $\times 10^{-9}$. In Fig. S3a, DIA_{Tot} is represented by the orange area.

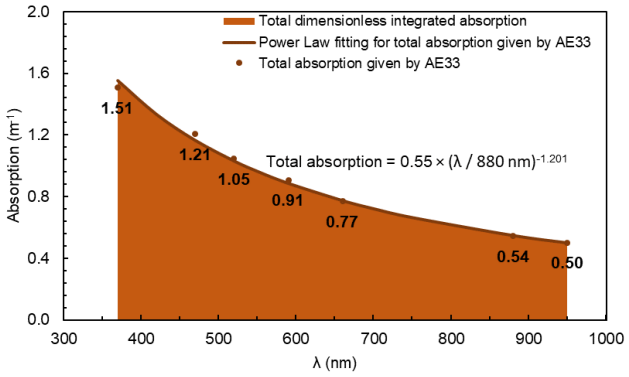

Figure S3a. Total absorptions (m^{-1}) given by AE33 at the seven wavelengths (brown marker), the power law fitting for the total absorption (brown line), and the DIA_{Tot} (orange area). The numbers in the graph are the total absorption coefficients (m^{-1}) given by AE33 for the individual wavelengths (370–950 nm).

For calculation of the DIA_{BC} of each experiment type, the b_{abs}(880 nm) value is determined as the average absorption coefficient at 880 nm. DIA_{BC} (shown as a grey area in Fig. S3b) is calculated by integrating Eq. (S3) over a wavelength range of 370 nm to 950 nm as shown in Eq. (S4). With the average b_{abs}(880 nm) of 0.54 m^{-1} for MCS, including all the different fuel types, the DIA_{BC} was 452.5×10^{-9} for MCS.

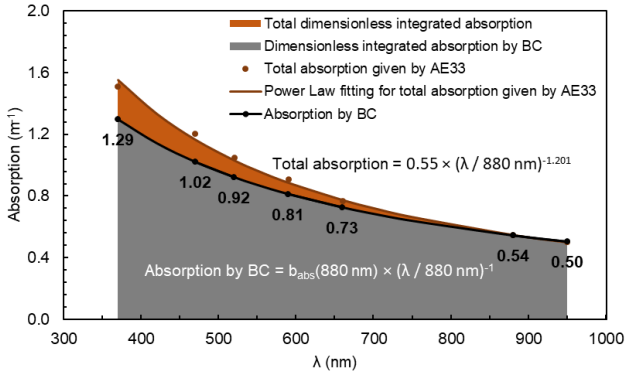

Figure S3b. In addition to Fig. S3a, the absorption by BC when AAE_{BC} = 1 is shown in a black line. The DIA_{BC} is represented with a grey area. The numbers in the graph are the absorption by BC (m^{-1}) at individual wavelengths (370–950 nm) calculated with AAE_{BC} = 1.

DIA_{BrC} is then calculated as the difference between DIA_{Tot} and DIA_{BC}. In Fig. S3c, DIA_{BrC} is represented as a yellowish-brown area. For MCS, the DIA_{BrC} value was 43.9×10^{-9}. The total contribution of BrC to the light absorption is then calculated as the ratio of DIA_{BrC} to DIA_{Tot}, resulting in $BrC_{370\text{-}950}$ of 8.9 % for MCS.

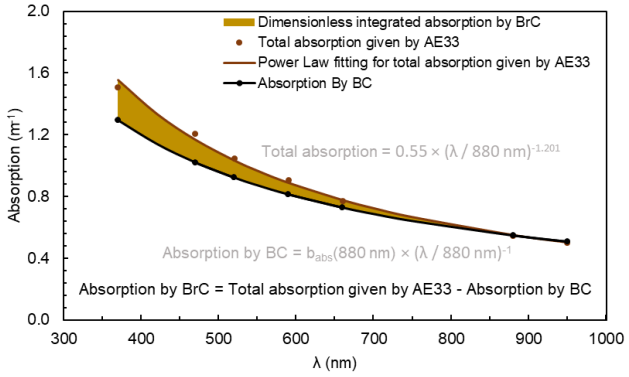

Figure S3c. The dimensionless integrated absorption (DIA_{BrC}), defined as the difference between DIA_{Tot} (Fig. S3a) and DIA_{BC} (Fig. S3b), is illustrated as the yellowish-brown area.

Table S3. The range of estimated relative uncertainty of $AAE_{470/950}$ in different combustions experiments. *Sauna stoves are presented as SSX_YY, where X represents different stoves (1-10) and YY represents the fuel moisture content (11-28 %).

Appliance	Abbrv.	Measurement site and date	fuel type	1 min average	Batch wise average	Whole experiment average
Modern masonry heater	MMH	ILMARI 2013	beech	0–179	0.1–2.1	0.1–0.8
			spruce	0–72	0.1–0.7	0.1–0.2
			birch	0–1206	0.4–6.3	0.3–2.1

Conventional masonry heater	CMH	SIMO 2019	birch	0–13352	0.9–10.9	1.8–3.9
Sauna stoves* (10 types)	SS1_11	SIMO 2018	birch	0–7118	0.4–8.9	1.6–3.8
	SS1_18		birch	0–11568	1.3–11.0	1.6–3.6
	SS2_17		birch	0–2925	1.4–8.1	2.0–3.8
	SS3_17		birch	0–8070	3.7–13.3	2.8–7.3
	SS4_11		birch	0–359917	10.4–76.0	12.2–34.0
	SS5_11		birch	0–4491	0.6–6.7	1.7–3.7
	SS6_11		birch	0–15870	3.0–7.6	2.9–3.8
	SS7_11		birch	0–11305	1.6–14.2	1.7–4.9
	SS8_11		birch	0–19396	3.6–13.8	2.5–8.1
	SS8_18		birch	0–450743	1.0–11.6	2.1–37.5
	SS8_28		birch	0–7520	0.6–11.5	1.9–2.4
	SS9_11		birch	0–34849	2.8–18.1	1.8–6.2
	SS10_11		birch	0–14026	1.2–11.9	0.8–7.0
Modern chimney stove	MCS	ILMARI 2016	pine	0–228	0.2–1.0	0.1–0.7
			spruce	0–173	0.1–0.6	0.1–0.5
		ILMARI 2021	beech	0–2000	0.3–8.9	0.4–4.3
			peat	0–1337	0.2–6.3	0.0–0.0
Pellet boiler	PB	ILMARI 2016	softwood pellets	0–272	0.0–0.3	0.0–0.3
Non-road diesel engine	NrDE	ILMARI 2016	diesel	0–104	0.0–0.3	0.1–0.1

Section S2 Uncertainty in the BrC fraction

The uncertainty in the relative contribution of BC and BrC to the absorption at the wavelengths measured by the aethalometer was derived based on the uncertainties in the instrument parameters. The total absorption at each wavelength measured by the aethalometer is given by Eq. S7 (Drinovec et al., 2015):

$$b_{abs,tot}(\lambda) = \frac{S(\frac{\Delta ATN_{880nm}}{100})}{F(1-Z)C(1-k_{\lambda}\times ATN_{\lambda})\Delta t} \quad \text{(S7)}$$

Where S, F, Z, and C are instrument-dependent constants for spot surface area, volumetric flow, leaking, and multiple scattering corrections, respectively. The absorption by BC is calculated for each wavelength from the attenuation at 880 nm using an $AAE_{BC} = 1$ (Eq. S8).

$$b_{abs,BC}(\lambda) = \frac{S(\frac{\Delta ATN_{880nm}}{100})}{F(1-Z)C(1-k_{880nm}\times ATN_{880nm})\Delta t} \times (\frac{\lambda}{880})^{-AAE_{BC}} \quad \text{(S8)}$$

For each wavelength, the relative fraction of absorption by BC is then given by the ratio of b_{abs}(BC, λ) to the total b_{abs} (Eq. S9).

$$BC(\%) = \frac{b_{abs,\,BC}(\lambda)}{b_{abs,\,tot}(\lambda)} = \frac{\frac{\Delta ATN_{880nm}}{1-k_{880nm}\times ATN_{880nm}}\times\left(\frac{\lambda}{880}\right)^{-1}}{\frac{\Delta ATN_{\lambda}}{1-k_{\lambda}\times ATN_{\lambda}}} = \frac{\Delta ATN_{880nm}}{1-k_{880nm}\times ATN_{880nm}} \times \frac{1-k_{\lambda}\times ATN_{\lambda}}{\Delta ATN_{\lambda}} \times \frac{880}{\lambda} \quad \text{(S9)}$$

and BrC by Eq. S10:

$$BrC(\%) = 1 - \frac{b_{abs,\,BC}(\lambda)}{b_{abs,\,tot}(\lambda)} = 1 - \frac{\Delta ATN_{880nm}}{1-k_{880nm}\times ATN_{880nm}} \times \frac{1-k_{\lambda}\times ATN_{\lambda}}{\Delta ATN_{\lambda}} \times \frac{880}{\lambda} \quad \text{(S10)}$$

The uncertainty function of the fraction of BC or BrC on each wavelength (Eq. S11) finally depends on six variables: $\Delta ATN_{880nm}, k_{880nm}, ATN_{880nm}, \Delta ATN_{\lambda}, k_{\lambda}, and\ ATN_{\lambda}$. Note that the absolute uncertainty is the same for both BC and BrC, while the relative uncertainty increases for the smaller quantity (typically BrC).

$$\delta f = \sqrt{\begin{array}{c}\left(\frac{\partial f}{\partial \Delta ATN_{880nm}}\right)^2 (\delta \Delta ATN_{880nm})^2 + \left(\frac{\partial f}{\partial k_{880nm}}\right)^2 (\delta k_{880nm})^2 + \left(\frac{\partial f}{\partial ATN_{880nm}}\right)^2 (\delta ATN_{880nm})^2 \\ + \left(\frac{\partial f}{\partial \Delta ATN_{\lambda}}\right)^2 (\delta \Delta ATN_{\lambda})^2 + \left(\frac{\partial f}{\partial k_{\lambda}}\right)^2 (\delta k_{\lambda})^2 + \left(\frac{\partial f}{\partial ATN_{\lambda}}\right)^2 (\delta ATN_{\lambda})^2\end{array}} \quad \text{(S11)}$$

For k_{λ}'s, arithmetic means of complete measurements were used. The uncertainty in k_{λ} (∂k_{λ}) was estimated as the SD during the corresponding whole experiment (typically in the order of 10^{-4} – 10^{-5}). Similarly to Helin et al. (2021), we simplified the uncertainty equation δf by assuming that uncertainty in the change in ATN is the same for all wavelengths and independent of time (Backman et al., 2017):

$$\delta \Delta ATN \approx \delta \Delta ATN_{\lambda} \approx \delta \Delta ATN_{880nm} \quad \text{(S12)}$$

and that the uncertainty in the attenuation (δATN) is equal to $\delta\Delta$ATN/√2. This leads to simplified uncertainty function (S13, further reordered in S14):

$$\delta f = \sqrt{\begin{array}{c}\left(\frac{\partial f}{\partial \Delta ATN_{880nm}}\right)^2 (\delta \Delta ATN)^2 + \left(\frac{\partial f}{\partial k_{880nm}}\right)^2 (\delta k_{880nm})^2 + \left(\frac{\partial f}{\partial ATN_{880nm}}\right)^2 \left(\delta \Delta ATN/\sqrt{2}\,\right)^2 \\ + \left(\frac{\partial f}{\partial \Delta ATN_{\lambda}}\right)^2 (\delta \Delta ATN)^2 + \left(\frac{\partial f}{\partial k_{\lambda}}\right)^2 (\delta k_{\lambda})^2 + \left(\frac{\partial f}{\partial ATN_{\lambda}}\right)^2 \left(\delta \Delta ATN/\sqrt{2}\,\right)^2\end{array}} \quad \text{(S13)}$$

$$\delta f = \sqrt{\left(\left(\frac{\partial f}{\partial \Delta ATN_{880nm}}\right)^2 + \frac{1}{2}\left(\frac{\partial f}{\partial ATN_{880nm}}\right)^2 + \left(\frac{\partial f}{\partial \Delta ATN_{\lambda}}\right)^2 + \frac{1}{2}\left(\frac{\partial f}{\partial ATN_{\lambda}}\right)^2\right)(\delta \Delta ATN)^2 + \left(\frac{\partial f}{\partial k_{880nm}}\right)^2 (\delta k_{880nm})^2 + \left(\frac{\partial f}{\partial k_{\lambda}}\right)^2 (\delta k_{\lambda})^2} \quad \text{(S14)}$$

where the partial derivatives are as follows:

$$\frac{\partial f}{\partial \Delta ATN_{880nm}} = \frac{1-k_{\lambda} \times ATN_{\lambda}}{\Delta ATN_{\lambda}(1-k_{880nm} \times ATN_{880nm})} \times \frac{880}{\lambda} \quad \text{(S15)}$$

$$\frac{\partial f}{\partial k_{880}} = \frac{\Delta ATN_{880nm} \times ATN_{880nm}(1-k_{\lambda} \times ATN_{\lambda})}{\Delta ATN_{\lambda}(1-k_{880nm} \times ATN_{880nm})^2} \times \frac{880}{\lambda} \quad \text{(S16)}$$

$$\frac{\partial f}{\partial ATN_{880nm}} = \frac{\Delta ATN_{880nm} \times k_{880}\,(1-k_{\lambda} * ATN_{\lambda})}{\Delta ATN_{\lambda}(1-k_{880nm} \times ATN_{880nm})^2} \times \frac{880}{\lambda} \quad \text{(S17)}$$

$$\frac{\partial f}{\partial \Delta ATN_{\lambda}} = -\frac{1-k_{\lambda} \times ATN_{\lambda}}{\Delta ATN_{\lambda}^2(1-k_{880nm} \times ATN_{880nm})} \times \frac{880}{\lambda} \quad \text{(S18)}$$

$$\frac{\partial f}{\partial k_{\lambda}} = -\frac{\Delta ATN_{880nm} \times ATN_{\lambda}}{\Delta ATN_{\lambda}(1-k_{880nm} \times ATN_{880nm})} \times \frac{880}{\lambda} \quad \text{(S19)}$$

$$\frac{\partial f}{\partial ATN_{\lambda}} = -\frac{\Delta ATN_{880nm} \times k_{\lambda}}{\Delta ATN_{\lambda}(1-k_{880nm} \times ATN_{880nm})} \times \frac{880}{\lambda} \quad \text{(S20)}$$

e resulting absolute uncertainties for the contribution of BrC and BC to the absorption at the seven aethalometer wavelengths are presented in Figure S4 for the different fuel-appliance pairs.

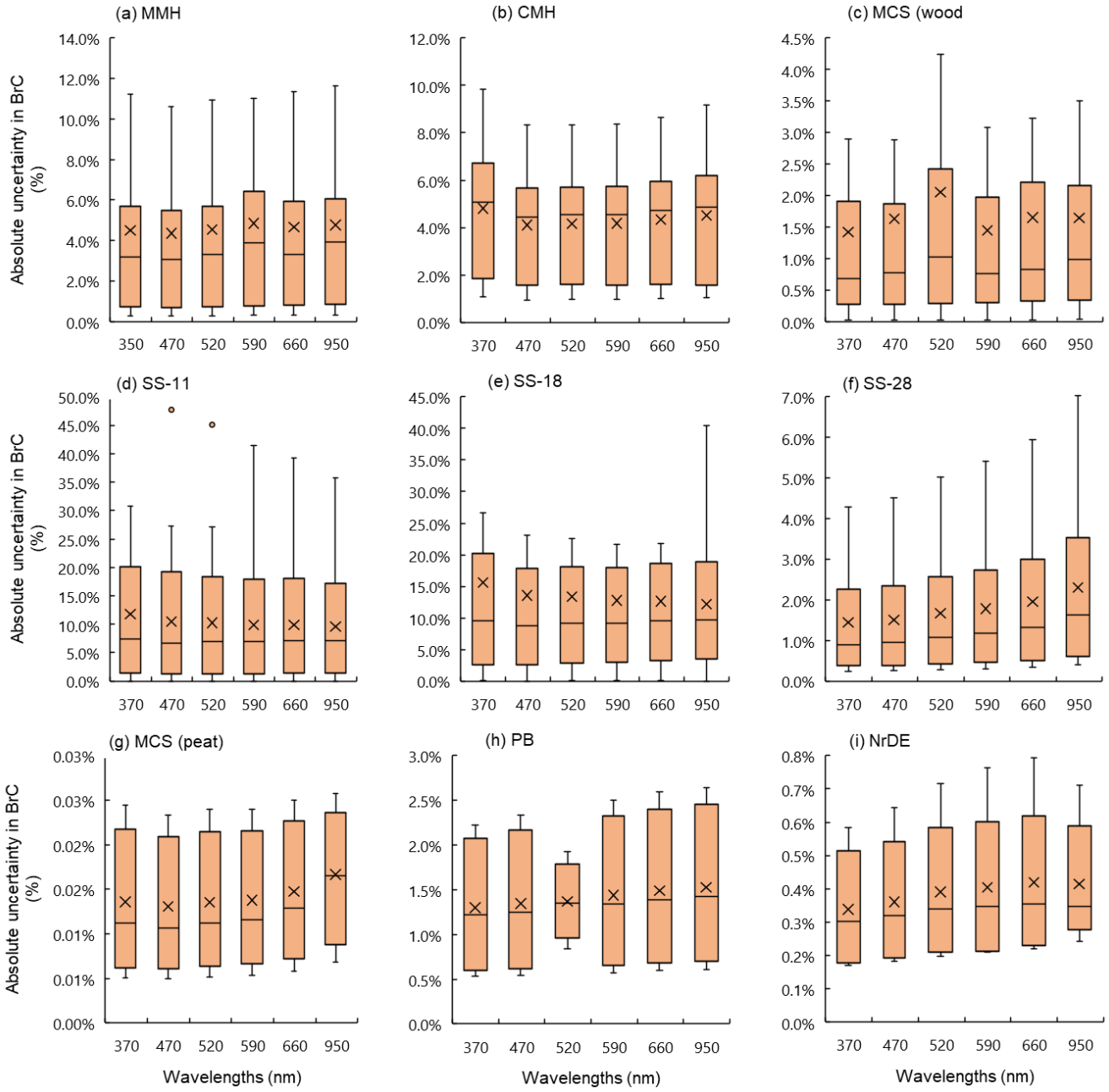

Figure S4. Absolute uncertainty in absorption by BrC (%) and BC based on two-wavelength measurements with $AAE_{BC} = 1$. The box edges show the 25th to 75th percentile range of experiment-wise averaged uncertainties, the horizontal line shows the 50th percentile and the whiskers indicate the 5th to 95th percentile range. '×' indicates the arithmetic mean of the uncertainties. The absolute uncertainties are calculated from the individual experimental days except for combustion peat in MCS, which is calculated from individual batch experiments.

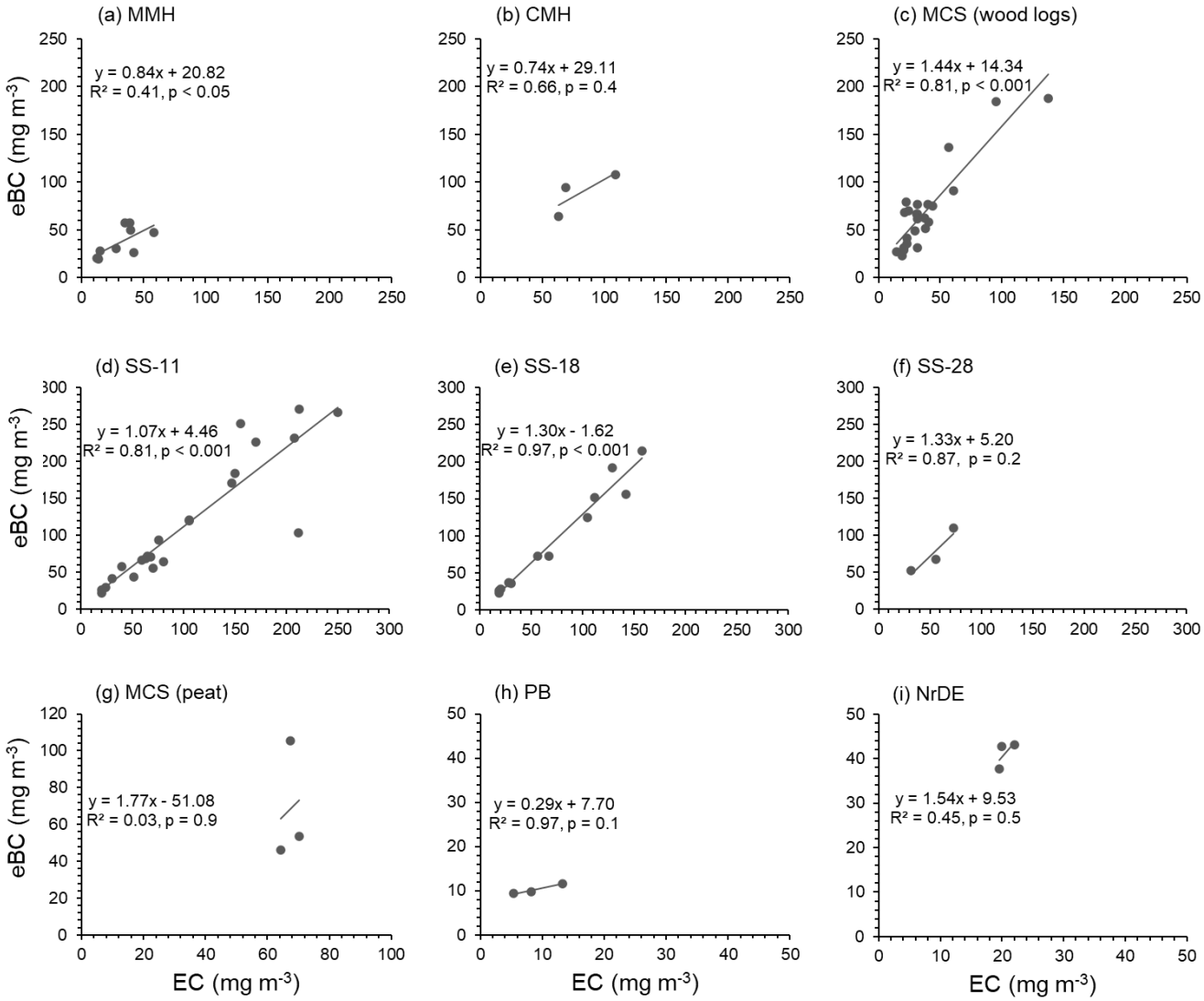

Figure S5. Comparison of the EC concentration (mg m^{-3}) (offline filter analysis) to the average eBC concentration (mg m^{-3}) (online optical measurements, AE33) in the raw gas conditions for a) MMH, b) CMH, c) MCS with wood logs, d) SS1 with birch logs with 11% moisture content, e) SS2 with birch logs with 18% moisture content, f) SS3 with birch logs with 28% moisture content, g) MCS with peat, h) PB, and i) non-road diesel engine. The solid line represents the linear regression with Pearson correlation coefficient of R) and significance of p (based on the F-value of the regression). EC measurement analysis for MMH, CMH, SS, PB, and the non-road diesel engine was performed using NIOSH 5040 thermal protocol while MCS was analyzed using IMPROVE-A protocol.

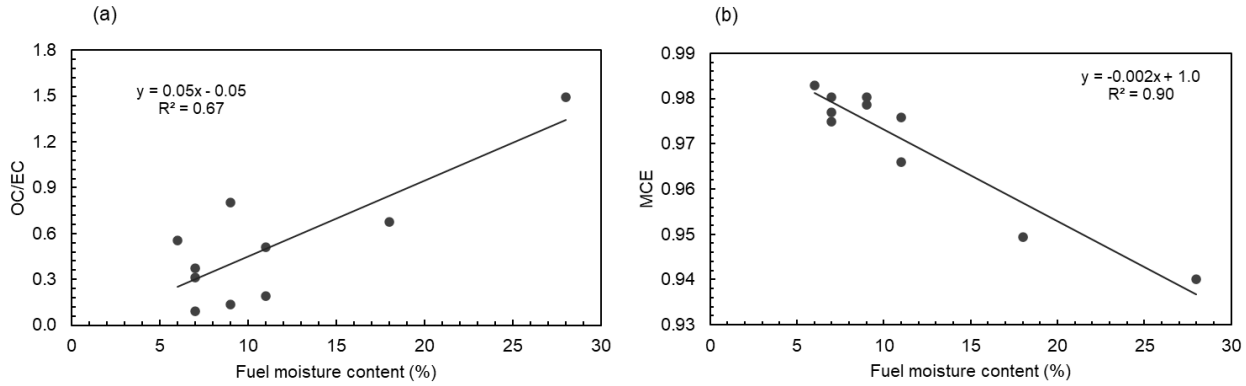

105

Figure S6. Relation between a) OC/EC and b) MCE with fuel moisture content for the averaged wood log fuel/appliance combinations.

Table S4. The particle number size distributions, $AAE_{470/950}$ (± SD of individual values), OC/EC ratio, and MAC_{880nm} (± SD of means) for different fuel-appliance combinations.

Appliances	Fuel types	Fuel moisture content	GMD (nm)	GSD	$AAE_{470/950}$	OC/EC	MAC_{880nm} ($m^2\ g^{-1}$)
MMH	Beech	9%	58.36	1.90	1.19 ± 0.40	0.14 ± 0.07	9.98 ± 4.13
	Spruce	7%	59.73	1.90	1.22 ± 0.19	0.31 ± 0.24	12.9 ± 1.25
	Birch	7%	66.95	1.95	1.00 ± 0.31	0.09 ± 0.04	9.00 ± 2.75
CMH	Birch	11%	97.40	1.92	1.19 ± 0.63	0.19 ± 0.05	8.41 ± 1.34
SS-11	Birch	11%	115.5	1.98	1.26 ± 0.18	0.51 ± 0.42	8.56 ± 1.80
SS-18	Birch	18%	128.3	2.01	1.34 ± 0.36	0.68 ± 0.31	10.0 ± 0.91
SS-28	Birch	28%	105.7	2.01	1.61 ± 0.47	1.49 ± 0.16	11.0 ± 1.45
MCS	Pine	6%	122.8	2.11	1.13 ± 0.20	0.55 ± 0.52	12.2 ± 2.05
	Spruce	7%	87.16	2.11	1.24 ± 0.21	0.37 ± 0.15	13.7 ± 2.80
	Beech	9%	81.64	2.00	1.29 ± 0.49	0.80 ± 0.62	15.0 ± 5.48
	Peat	18%	64.36	1.86	1.18 ± 0.83	0.17 ± 0.05	7.88 ± 3.01
PB	Softwood Pellet	7%	57.52	2.03	1.24 ± 0.12	0.19 ± 0.09	8.16 ± 2.84
NrDE	Diesel		44.30	1.84	1.02 ± 0.05	0.10 ± 0.01	15.6 ± 0.75

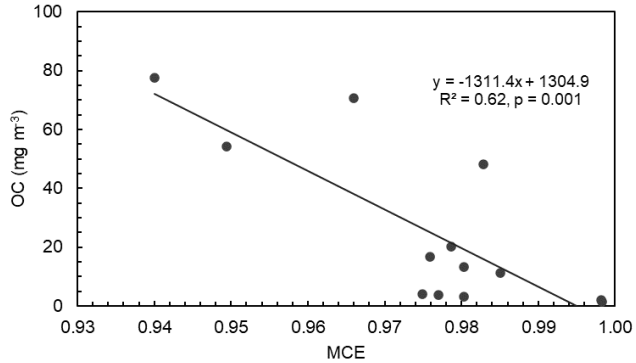

Figure S7. Relation between OC (mg m^{-3}, in raw gas conditions) and MCE for the wood log combustion appliances (average of fuel/appliance types).

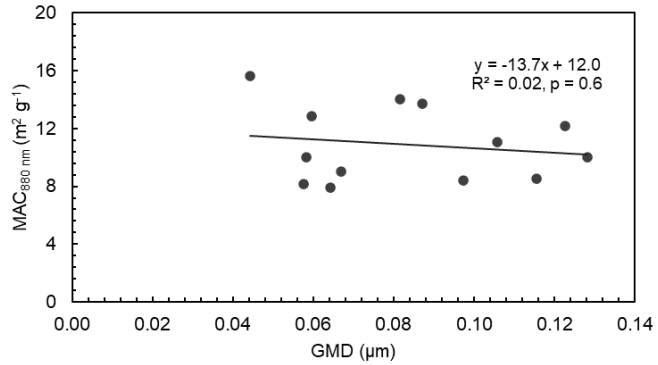

Figure S8. Relation between $MAC_{880\ nm}$ ($m^2\ g^{-1}$) and GMD (nm) for the wood combustion appliances (average of fuel/appliance types).

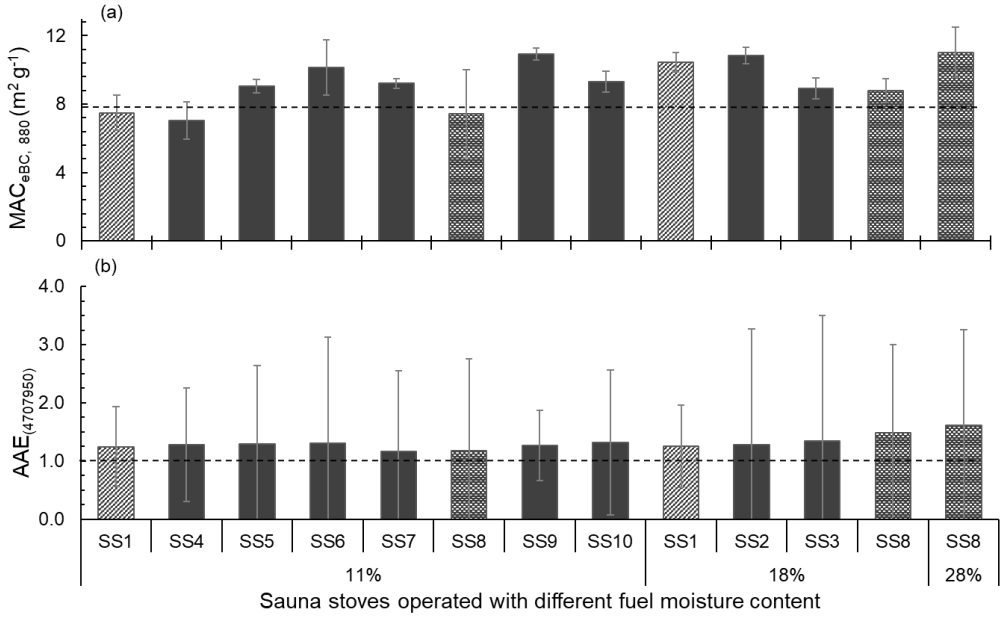

Figure S9. Optical properties of emissions from sauna stoves 1-10 given as SS1 to S10 operated with wood logs with different fuel moisture content (11%, 18%, and 28 %). a) $MAC_{eBC,880nm}$ ($m^2\ g^{-1}$) (± SD) and b)$AAE_{470/950}$ (± SD) for stoves 1-10. The bars with patterns indicate the same stoves (SS1 and SS8) with fuels having different moisture content. The data are partially published in Tissari et al., (2019).

Table S5. Optical properties (± SD) of the emissions from sauna stoves 1-10 given as SS1 to S10 operated with birch logs with different fuel moisture contents.

Appliances	Fuel moisture content (%)	$AAE_{470/950}$	MAC_{880nm}	Total abs by BC (%) (AAE_{BC} = 1)	Total abs by BrC (%) (AAE_{BC} = 1)
SS1	11	1.2 ± 0.7	7.5 ± 1.0	94.8	5.17
SS4	11	1.3 ± 1.0	7.0 ± 1.1	91.4	8.63
SS5	11	1.3 ± 1.3	9.1 ± 0.4	91.7	8.34
SS6	11	1.3 ± 1.8	10 ± 1.6	91.6	8.42
SS7	11	1.2 ± 1.4	9.2 ± 0.3	98.0	1.98
SS8	11	1.2 ± 1.6	7.4 ± 2.6	96.9	3.11
SS9	11	1.3 ± 0.6	11 ± 0.4	94.2	5.83
SS10	11	1.3 ± 1.2	9.3 ± 0.6	88.8	11.2
SS1	18	1.3 ± 0.7	10 ± 0.6	90.2	9.81
SS2	17	1.3 ± 2.0	11 ± 0.5	90.8	9.17
SS3	17	1.3 ± 2.2	8.9 ± 0.6	89.8	10.2
SS8	18	1.5 ± 1.5	8.8 ± 0.7	82.5	17.5
SS8	28	1.6 ± 1.6	11 ± 1.5	77.3	22.7

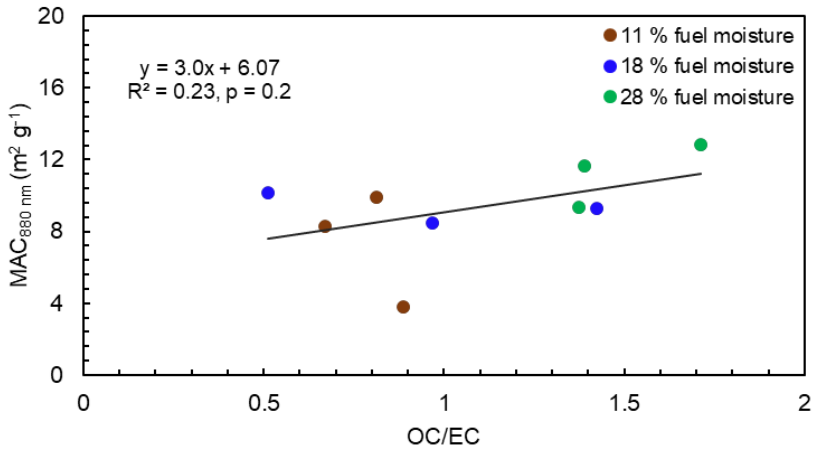

Figure S10. Relation between $MAC_{880\ nm}$ ($m^2\ g^{-1}$) and OC/EC for SS8, utilizing fuel with three different moisture content.

Table S6. The contribution of BC ($BC_{370-950}$) and BrC ($BrC_{370-950}$) to the total absorption with AAE_{BC} =1 for different fuel-appliance combinations, along with the contribution of BrC to the absorption at different wavelengths measured by the AE33.

Appliance	Fuel type	Fuel Moisture content	$BC_{370-950}$ (%)	$BrC_{370-950}$ (%)	Contribution of BrC to the absorption at individual wavelengths (%)				
					370 nm	470 nm	520 nm	590 nm	660 nm
MMH	Beech	9%	93.2	6.78	7.73	12.7	9.33	7.84	7.93
	Spruce	7%	91.1	8.90	14.1	15.2	10.8	9.14	8.97
	Birch	7%	98.7	2.97	-3.28	3.59	1.31	1.84	3.82
CMH	Birch	11%	98.5	1.50	-7.44	8.00	6.03	5.21	1.10
SS-11	Birch	11%	94.7	5.34	5.05	12.9	9.48	7.48	3.08
SS-18	Birch	18%	90.3	9.68	17.4	17.4	13.9	11.1	4.91
SS-28	Birch	28%	79.2	20.8	36.2	33.4	25.8	20.6	12.2
MCS	Pine	6%	95.6	4.37	5.30	8.63	6.73	6.32	3.36
	Spruce	7%	90.1	9.92	17.7	17.1	13.0	11.0	6.65
	Beech	9%	89.8	10.2	16.6	18.1	14.2	12.3	6.53
	Peat	18%	94.0	5.98	4.78	11.4	9.52	9.03	4.52
PB	Softwood Pellet	7%	90.3	9.67	19.4	16.0	10.8	8.61	4.45
NrDE	Diesel		99.3	0.66	5.04	3.14	-0.82	-1.32	-2.66

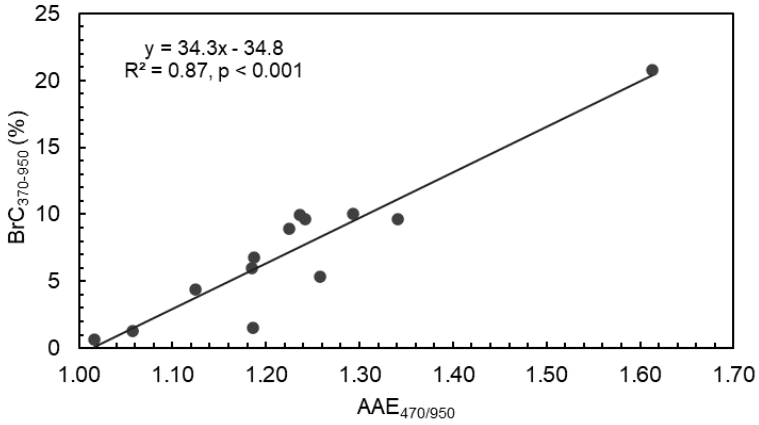

Figure S11. Relation between absorption by $BrC_{370-950}$ (%) and $AAE_{470/950}$.

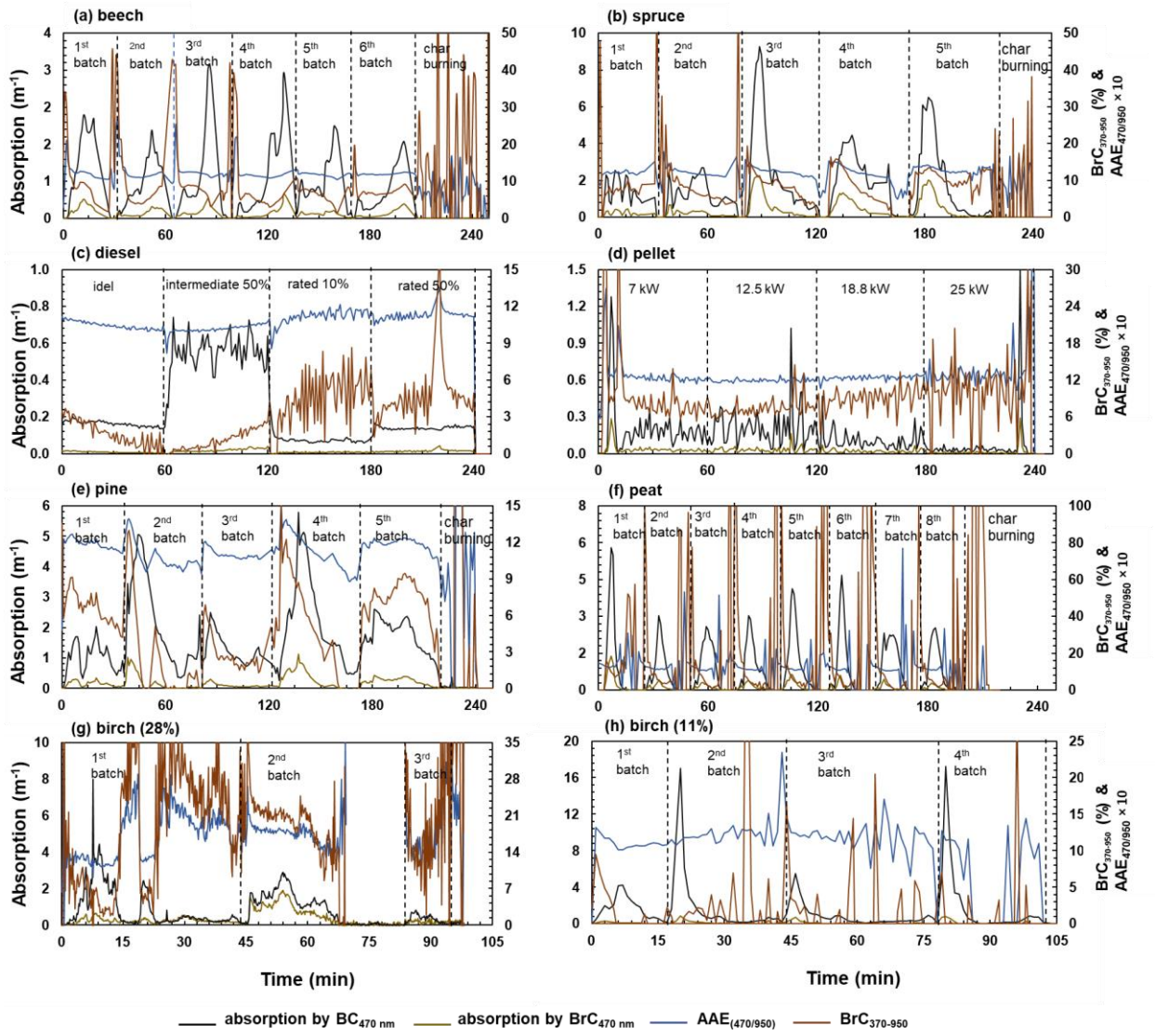

Figure S12. Examples of the time series for absorption by BC (black) and BrC (yellow) (m^{-1} in raw exhaust gas concentrations) at 470 nm along with $AAE_{470/950}$ values (blue) and $BrC_{370\text{-}950}$ total absorption (brown) (%) for combustion experiments using different fuel types in following combustion appliances: a) MMH, b) MCS, c) non-road diesel engine, d) PB, e) MCS, f) MCS, g) SS, and h) CMH. In (g), $AAE_{470/950}$ and $BrC_{370\text{-}950}$ are not shown for the ember phase (69–84 min) due to the low PM emission.

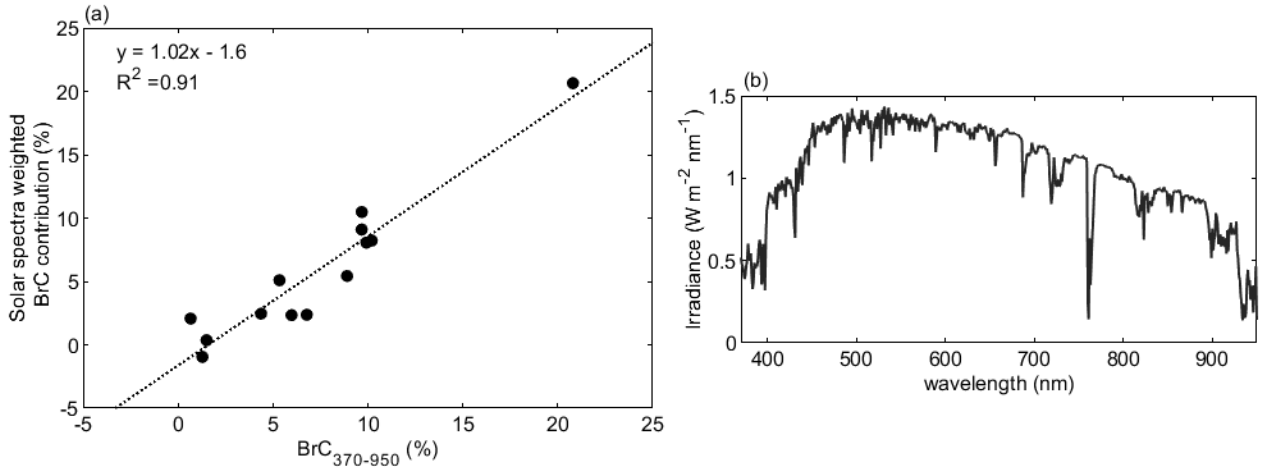

Figure S13. The relation of $BrC_{370\text{-}950}$ to the solar-spectra weighted contribution of brown carbon to light absorption in the range of 370 nm-950 nm (a), with the ASTM G173-03 solar reference spectra (direct + circumsolar) applied for the estimation shown in (b).

Section S3 Impact of the choice of AAE_{BC} on the contribution of BrC to the total absorption

The contribution of BrC to the total absorption ($BrC_{370\text{-}950}$) depends on the choice of AAE_{BC}. Typically, AAE_{BC} =1 is used; if the actual AAE_{BC} differs from this, the change in the determined $BrC_{370\text{-}950}$ is described as:

$$change\ in\ the\ BrC_{370-950nm} = \frac{1-R\times BC_{1,}-BrC_{1,\%}}{BrC_{1,\%}} \quad \text{(S21)}$$

where, BC_1 and BrC_1 are the fractional contributions of BC and BrC to the total absorption, respectively, with AAE_{BC} =1, so that $BC_1 + BrC_1 = 1$. R is the ratio of the BC absorption with the alternative AAE (AAE_2) to that with AAE_{BC} =1. In the range of 370 – 950 nm, the ratio R can be derived from the definition of BC as:

$$R = \frac{\int_{370\ nm}^{950\ nm} b_{abs,880nm\times}\left(\frac{\lambda}{880}\right)^{-AAE_2} d\lambda}{\int_{370\ nm}^{950\ nm} b_{abs,880nm\times}\left(\frac{\lambda}{880}\right)^{-1} d\lambda} = \frac{880^{AAE_2-1}\times\left(950^{-AAE_2+1}-370^{-AAE_2+1}\right)}{(-AAE_2+1)\times\ln\left(\frac{950}{370}\right)} \quad \text{(S22)}$$

The sensitivity of $BrC_{370\text{-}950}$ on the AAE depends on the amount of BrC in the exhaust, as illustrated in Fig. S14 for AAE_{BC}s 0.9 and 1.1.

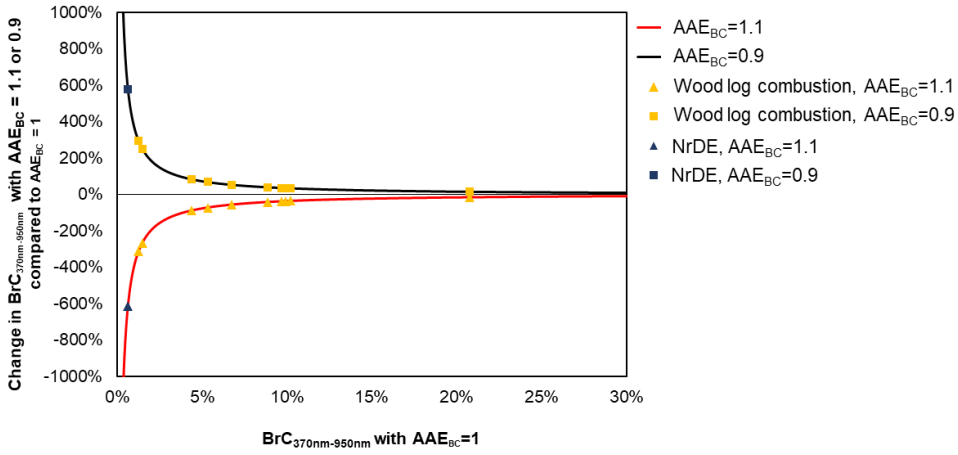

Figure S14. Change in the contribution of BrC to the total absorption in the wavelength range 370 nm - 950 nm ($BrC_{370-950}$) when AAE_{BC} is changed from 1.0 to 0.9 or 1.1.

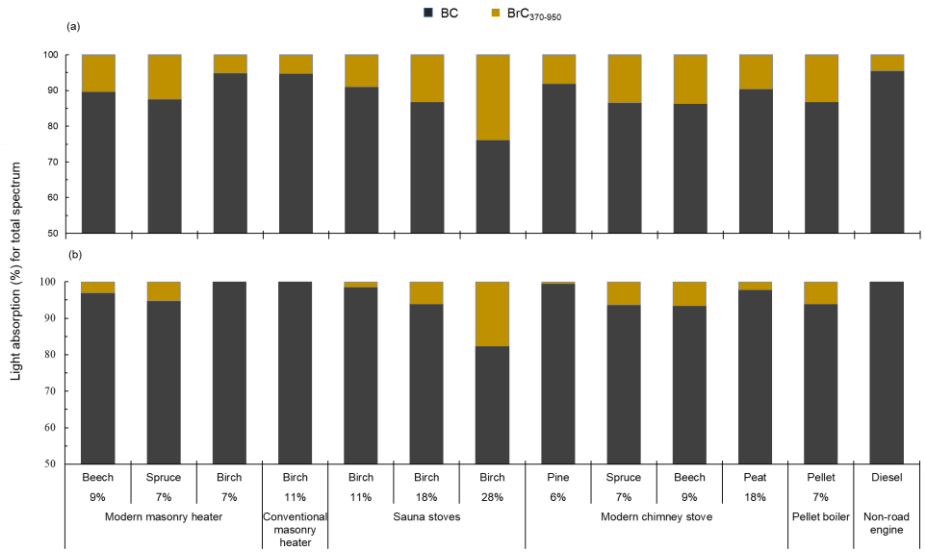

Figure S15. Change in $BrC_{370-950}$ contribution for different fuel types and combustion appliances when a) AAE = 0.9 and b) AAE = 1.1. The percentages shown indicate the fuel moisture content.

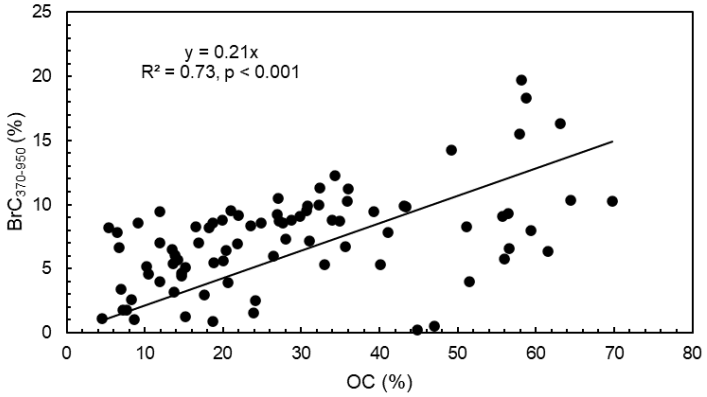

Figure S16. Relation between OC (%) and total $BrC_{370\text{-}950}$ (%) for individual experiments.

References

155 Backman, J., Schmeisser, L., Virkkula, A., Ogren, J. A., Asmi, E., Starkweather, S., Sharma, S., Eleftheriadis, K., Uttal, T., Jefferson, A., Bergin, M., Makshtas, A., Tunved, P., and Fiebig, M.: On Aethalometer measurement uncertainties and an instrument correction factor for the Arctic, Atmos. Meas. Tech., 10, 5039–5062, 10.5194/AMT-10-5039-2017, 2017.

Drinovec, L., Močnik, G., Zotter, P., Prévôt, A. S. H., Ruckstuhl, C., Coz, E., Rupakheti, M., Sciare, J., Müller, T., Wiedensohler, A., and Hansen, A. D. A.: The "dual-spot" Aethalometer: An improved measurement of aerosol black carbon
160 with real-time loading compensation, Atmos. Meas. Tech., 8, 1965–1979, 10.5194/amt-8-1965-2015, 2015.

Helin, A., Virkkula, A., Backman, J., Pirjola, L., Sippula, O., Aakko-Saksa, P., Väätäinen, S., Mylläri, F., Järvinen, A., Bloss, M., Aurela, M., Jakobi, G., Karjalainen, P., Zimmermann, R., Jokiniemi, J., Saarikoski, S., Tissari, J., Rönkkö, T., Niemi, J. V., and Timonen, H.: Variation of Absorption Ångström Exponent in Aerosols From Different Emission Sources, J. Geophys. Res. Atmos., 126, e2020JD034094, 10.1029/2020JD034094, 2021.

165 Tissari, J., Väätäinen, S., Leskinen, J., Savolahti, M., Lamberg, H., Kortelainen, M., Karvosenoja, N., and Sippula, O.: Fine particle emissions from sauna stoves: Effects of combustion appliance and fuel, and implications for the Finnish emission inventory, Atmosphere (Basel)., 10, 775, 10.3390/ATMOS10120775, 2019.